

CMB AND LARGE SCALE STRUCTURE AS A TEST OF MIXED MODELS WITH $n > 1$

Elena Pierpaoli¹ and Silvio Bonometto^{2,3}

¹*SISSA – International School for Advanced Studies, Via Beirut 2/4, I34013 Trieste, Italy*

²*Department of Physics of the University, Via Celoria 16, Milano, Italy*

³*INFN – Sezione di Milano*

Accepted 1997 ** *. Received 1997 ** **; in original form 1997 ** **

ABSTRACT

We compute CBR anisotropies in mixed models with different hot components, including neutrinos or volatile HDM arising from the decay of heavier particles. The CBR power spectra of these models exhibit a higher doppler peak than CDM, and the discrepancy is even stronger in volatile models when the decay gives rise also to a neutral scalar.

CBR experiments, together with Large Scale Structure (LSS) data, are then used to constrain the space parameter of mixed models, when values of the primeval spectral index $n > 1$ are also considered. Even if $n > 1$ is allowed, however, LSS alone prescribes that $\Omega_h \lesssim 0.30$.

LSS can be fitted by taking simultaneously a low derelativization redshift z_{der} (down to $\simeq 600$) and a high n , while CBR data from balloon–borne experiment cause a severe selection on this part of the parameter space. In fact, while late derelativization and $n > 1$ have opposite effects on the fluctuation spectrum $P(k)$, they sum their action on the angular spectrum C_l . Henceforth $n \gtrsim 1.3$ seems excluded by balloon–borne experiment outputs, while a good fit of almost all CBR and LSS data is found for Ω_h values between 0.11 and 0.16, $n \sim 1.1$ and $z_{der} \sim 2000$ –5000. A smaller n is allowed, but z_{der} should never be smaller than $\simeq 1200$.

Key words: dark matter:decaying particles, dark matter: massive neutrinos, large scale structure of the Universe, cosmic microwave background: anisotropies.

1 INTRODUCTION

Anisotropies in the cosmic background radiation (CBR) are a strong potential source of information on the cosmological model. Unfortunately, anisotropy observations are hard and significant measures were obtained only recently. As a matter of fact, the theory of CBR anisotropies is well understood (see, e.g., Hu & Sugiyama 1995 and references therein) and public numerical codes allow to calculate the expected anisotropies for a wide range of cases (Seljak & Zaldarriaga 1996). It is then easy to see that CBR anisotropies depend on all the ingredients that define a cosmological model: the background metric, the substance mix and the primeval fluctuation spectrum. Several authors used available codes to predict CBR features for suitable ranges of model parameters. However, within the range of models consistent with

the inflationary paradigm, not enough attention, in our opinion, has been devoted yet to mixed models. Anisotropies expected for them were calculated by Ma & Betschinger (1995), De Gasperis et al. (1995), Dodelson et al. (1996), but parameter choices were restricted to cases for which anisotropies only marginally differ from the standard CDM case. Here we plan to extend the analysis to a wider set of mixed models including those for which a greater discrepancy from standard CDM can be expected and, in particular, models with primeval spectral index $n > 1$ and late derelativization of the hot component. If hot dark matter (HDM) is made of massive ν 's, there is a precise constraint between its density parameter (Ω_h) and its derelativization redshift (z_{der}):

$$\Omega_h \simeq 0.68(z_{der}/10^4)(g_\nu/6) \quad (1.1)$$

(see eqs. 2.3–2.4 below; g_ν is the number of ν spin states). Henceforth, in order to have $\Omega_h \gtrsim 0.10$ –0.15, z_{der} cannot be lower than ~ 2000 , even for $g_\nu = 6$. In order to have lower

† E-mail: pierpa@sissa.it;
bonometto@mi.infn.it

z_{der} and/or greater Ω_h , HDM must arise from the decay products of heavier particles. In fact, decay products have extra kinetic energy arising from mother particle mass energy and therefore have a later z_{der} . Several authors considered such scenario, assuming the decay of a heavier neutrino into a lighter one (Bond & Efstathiou 1991, Dodelson et al. 1994, White et al. 1995, McNally & Peacock 1995, Ghizzardi & Bonometto 1996), and there are recent attempts of constraining it using CBR data (Hannestad 1998). However, a wider range of models give rise to similar pictures, *e.g.*, if metastable supersymmetric particles decay into lighter ones (Bonometto et al., 1994; Borgani et al. 1996). In a number of recent papers HDM arising from decays was called *volatile*, to stress its capacity to grant a later derelativization, which weakens its contribution to the formation of inhomogeneities.

CBR anisotropies were first detected by the COBE–DMR experiment (Smoot et al. 1992). The angular scales observed by COBE were rather wide ($\simeq 7^\circ$) and allowed to inspect a part of the spectrum which is almost substance independent. Nevertheless, COBE measurement provide the normalization of density fluctuations out of the horizon, and fair constraints on the primeval spectral index n (Bennet et al. 1996). More recent balloon–borne and ground based experiments investigated CBR fluctuations on scales comparable with the horizon scale at recombination. In the standard CDM model, on these scales, one expects the first doppler peak and, unlike what happens on larger scales, anisotropies are related both to the spectral index n and to substance mix. In principle, these scale are the best ones to test mixed models, as on even smaller scales ($l \gtrsim 500$ see below) the CBR spectrum can be distorted by other effects, like reionization and lensing.

The degree scale measurements currently available seem to have detected the doppler peak at a fair angular scale, but with an amplitude higher than expected in a standard CDM scenario with $n = 1$ (Scott et al. 1995, de Bernardis et al. 1997). An analysis of such outputs seems to exclude low values of the density parameter $\Omega = \rho/\rho_{cr}$ (Hancock et al. 1998, Bartlett et al. 1998). Here ρ is the present average density in the Universe and $\rho_{cr} = 3H^2/8\pi G$ depends on the value of the Hubble parameter $H = h 100 \text{ km s}^{-1} \text{ Mpc}^{-1}$. Furthermore, Lineweaver (1997) and Lineweaver & Barbosa (1998) outline that observed anisotropies are still too large to agree with CDM and $\Omega = 1$ unless $h \simeq 0.3$. Alternative causes for such greater fluctuations can be $n > 1$ or a cosmic substance comprising a substantial non–CDM component.

A number of large scale structure (LSS) observables are obtainable from the linear theory of fluctuation growing. A wide range of mixed models predict fair values for them. Tests of non linear features were also performed through N–body simulations (see *e.g.* Ghigna et al. (1997) and references therein). Although some technical aspects of mixed model simulations are still questionable, one can state that suitable DM mixtures allow to fit LSS data from 1 to 100 Mpc, almost up to scales covered by the current CBR experiments, so that a simultaneous analysis of CBR anisotropies and LSS allow complementary tests of the models.

It ought to be outlined that $n > 1$ and a hot component have a partially compensating effect on LSS and, in a previous paper (Bonometto & Pierpaoli 1998, hereafter BP; see also Lucchin et al. 1996, Liddle et al. 1996), we discussed

how they could be combined to obtain a fit with LSS data. On CBR fluctuations, instead, they add their effects and a quantitative analysis is needed to see how far one can go from both $n = 1$ and pure CDM. Most of this paper is focused on such analysis and on the tools needed to perform it.

In particular, let us outline that public codes, like CMB–FAST, cannot predict CBR anisotropies for mixed models with a hot component of non–thermal origin. A part of this work, therefore, required a suitable improvement of current algorithms.

In this work only models with $\Lambda = 0$, $h = 0.5$ and $\Omega = 1$ are considered. The *cosmic substance* is fixed by the partial density parameters: $\Omega_b = \rho_b/\rho_{cr}$ for baryons, $\Omega_c = \rho_c/\rho_{cr}$ for cold–dark–matter (CDM), Ω_h and z_{der} (see below) for HDM. Here we shall also distinguish between HDM made of massive ν 's (*neutrino* models) and HDM arising from heavier particle decay (*volatile* models). The relation between the nature of HDM and the amount of sterile massless components (SMLC hereafter) needs also to be discussed (in standard CDM, SMLC is made by 3 massless ν 's).

Early deviations from homogeneity are described by the spectrum

$$P_\Psi(k) = A_\Psi x^3 (xk)^{n-4} \quad (1.1)$$

($x = x_o - x_{rec}$ is the distance from the recombination band, as x_o is the present horizon radius). Here $k = 2\pi/L$ and L is the comoving length–scale. Models with $1 \leq n \leq 1.4$ were considered. In Appendix A we review which kinds of inflationary models are consistent with such n interval.

Section 2 is dedicated to a brief discussion on the different kinds of hot dark matter that could lead to a mixed dark matter scenario. In section 3 we analyze the CBR spectrum of such models, distinguishing between the effects due to the SMLC and those due to the actual phase–space distributions of the hot particles and discussing how current algorithms need to be modified to provide CBR anisotropies for volatile models. We then perform an analysis of the parameter space: models are preselected according to LSS constraints related to the linear theory. This selection is based on BP results, whose criteria will be briefly reviewed (section 4). BP results, however, were restricted to the case $\Omega_b = 0.1$. Here we shall inspect a greater portion of the parameter space, by considering also models with $\Omega_b = 0.05$, allowing for a substantial dependence of the CBR power spectrum on the baryon abundance. Section 5 is dedicated to a comparison of the CBR spectra with current available data, and to the final discussion.

2 DARK MATTER MIX

The *substance* of mixed models can be classified according to their behaviour when galactic scales (10^8 – $10^{12} M_\odot$) enter the horizon. Particles already non–relativistic are said *cold*. Their individual masses or energy distributions do not affect cosmological observables. *Tepid* or *warm* components (see, *e.g.* Pierpaoli et al., 1998) become non–relativistic while galactic scales enter the horizon. *Hot* component(s), instead, become non–relativistic after the latter scale has entered the horizon. Neutrinos, if massive, are a typical hot component. They were coupled to radiation for $T > T_{\nu,dg} \sim 900 \text{ keV}$.

If their mass $m \ll T_{\nu,dg}$, their number density, at any $T < T_{\nu,dg}$, is $n_\nu = (3\zeta(3)/4\pi^2)g_\nu T_\nu^3$ (after electron annihilation $T_\nu = T_{\nu,dg}[a_{\nu,dg}/a(t)] = (4/11)^{1/3}T$, where T is radiation temperature) and their momentum distribution (normalized to unity) reads

$$\Phi_\nu(p, t) = \frac{2}{3\zeta(3)} \frac{(p^2/T_\nu^3)}{\exp[p/T_\nu(t)] + 1} \quad (2.1)$$

also when $p \ll m$. Henceforth, when $T \ll m$, their distribution is not *thermal*, although its shape was originated in thermal equilibrium. Notice that, for high p , Φ_ν is cut off as $\exp(-p/T_\nu)$.

Using the distribution (2.1) we can evaluate

$$\langle p \rangle = (7\pi^4/180\zeta(3))T_\nu = 3.152 T_\nu . \quad (2.2)$$

If we define z_{der} as the redshift for which $\langle p \rangle = m$, eq. (2.2) tells us that z_{der} occurs when $T_\nu = 0.317 m$. In the following we shall use the parameter $d = 10^4/z_{der}$, which normalizes z_{der} at a value (10^4) in its expected range. At $z = 10^4$, photons and CDM would have an equal density in a pure CDM model with $h = 0.5$ and a present CBR temperature $T_o = 2.7333$ K. Henceforth, such redshift is in the range where we expect that relativistic and non-relativistic components have equal density (equivalence redshift: z_{eq}); besides of photons and SMLC, it is possible that HDM contributes to the relativistic component at z_{eq} . Its value, in different models, is given by eq. (2.11), herebelow. In general, we shall normalize T_o at the above value (which is well inside 1σ in respect to data) and define $\theta = T_o/2.7333$ K.

For neutrinos of mass m ,

$$d = 5.2972 \cdot 4h^2/(m/\text{eV}) , \quad (2.3)$$

while

$$\Omega_h = 2.1437 \cdot 10^{-2} g_\nu(m/\text{eV})\theta^3/4h^2 . \quad (2.4)$$

Let us now compare these features with those of a volatile model, where the hot component originates in the decay of heavier particles X (mass m_X), decoupled since some early time t_{dg} (see also Pierpaoli & Bonometto 1995, and Pierpaoli et al. 1997). If the temperature $T_{dg} \ll m_X$, such hot component may have a number density much smaller than massive neutrinos. Let $N_{X,dg}$ be the heavy particle comoving number density at decoupling. At $t \gg t_{dg}$ their comoving number density reads:

$$N_X(t) = N_{X,dg} \exp[-(t - t_{dg})/\tau_{dy}] \quad (2.5)$$

with $t_{dg} \ll \tau_{dy}$ (decay time). Assuming a two-body decay process $X \rightarrow v + \phi$, into a light (*volatile*) particle v (mass $m \ll m_X$) and a massless particle ϕ , it is shown that the volatile distribution, at $t \gg \tau_{dy}$, reads

$$\Phi_v(p, t) = 2(Q/p) \exp(-Q) , \quad (2.6)$$

where

$$Q = p^2/\tilde{p}^2 \text{ and } \tilde{p} = (m_X/2)[a_{dy}/a(t)] \quad (2.7)$$

provided that X 's, before they decay, never attain a density exceeding relativistic components causing a temporary matter dominated expansion.

At high p , the distribution (2.6) is cutoff $\propto \exp[-(p^2/\tilde{p}^2)]$ and this is true also if this temporary regime occurs.

In BP it is shown that, if the massless particle ϕ is a

photon (γ), such temporary expansion can never occur in physically relevant cases, which must however satisfy the restriction $\Omega_h d \ll 1$. This limitation does not hold if ϕ is a massless scalar as is expected to exist in theories where a global invariance is broken below a suitable energy scale (examples of such particles are *amilons* and *majorons*).

Using the distribution (2.6), it is easy to see that the average

$$\langle p \rangle = (\sqrt{\pi}/4)m_X a_{dy}/a(t) = \tilde{p}\sqrt{\pi}/2 \quad (2.8)$$

and v 's will therefore become non relativistic when $\tilde{p} = 2m/\sqrt{\pi}$; henceforth

$$\tilde{p} = 2 \cdot 10^4 z_{md}/\sqrt{\pi} \quad (2.9)$$

can be used in the distribution (2.6), instead of eq. (2.7).

If ϕ 's are sterile scalars and the decay takes place after BBNS, they will contribute to SMLC and affect CBR and LSS just as extra massless neutrino states.

Let us recall that, in the absence of X decay, the ratio $\rho_\nu/\rho_\gamma = 0.68132(g_\nu/6) \equiv w_o$. X decay modifies it, turning g_ν into an effective value

$$g_{\nu,eff} = g_\nu + (16/7)(11/4)^{4/3}\Omega_h d \quad (2.10)$$

In particular, ϕ 's lower the *equivalence* redshift. For $d(1 - \Omega_h) > 1 + w_o$, also v 's are still relativistic at equivalence. Accordingly, the equivalence occurs at either

$$\bar{z}_{eq} = \frac{4h^2}{\theta^4} \frac{10^4}{1 + w_o + \Omega_h d} \quad \text{or} \quad \bar{z}_{eq} = \frac{4h^2}{\theta^4} \frac{10^4(1 - \Omega_h)}{1 + w_o + 2\Omega_h d} \quad (2.11)$$

in the former and latter case, respectively.

Volatile models, as well as neutrino models, can be parametrized through the values of Ω_h and d . However, at given Ω_h , the latter ones are allowed only for discrete d values (notice that such d values are independent of h and can be only marginally shifted by changing θ). The former ones, instead, are allowed for a continuous set of d values. This can be seen in fig. 1, which is taken from BP, where more details on volatile models can be found. In fig. 1 we also show which models are consistent with LSS constraints and COBE quadrupole data, for various $n > 1$. Such constraints will be briefly discussed in the next section. In general, they are fulfilled for a part of the allowed Q values. Fig. 1 also shows that there is a large deal of mixed models with low z_{der} which are allowed by LSS data and are not consistent with HDM made of massive ν 's.

In this article we shall show that a portion of this extra parameter space seems however forbidden by CBR constraints.

3 THE RADIATION POWER SPECTRUM

To describe the evolution of radiation anisotropies in an expanding Universe, it is convenient to write the metric in the form

$$ds^2 = a^2(\tau)[(1 + 2\Psi)d\tau^2 - (1 - 2\Phi)\gamma_{\alpha\beta}dx^\alpha dx^\beta] . \quad (3.1)$$

in the conformal newtonian gauge. Here x^α (components of the vector \vec{x}) are space coordinates, τ is the conformal time, $a(\tau)$ is the scale factor and $\gamma_{\alpha\beta}$ gives the spatial part of the metric tensor in the homogeneity limit. The deviation

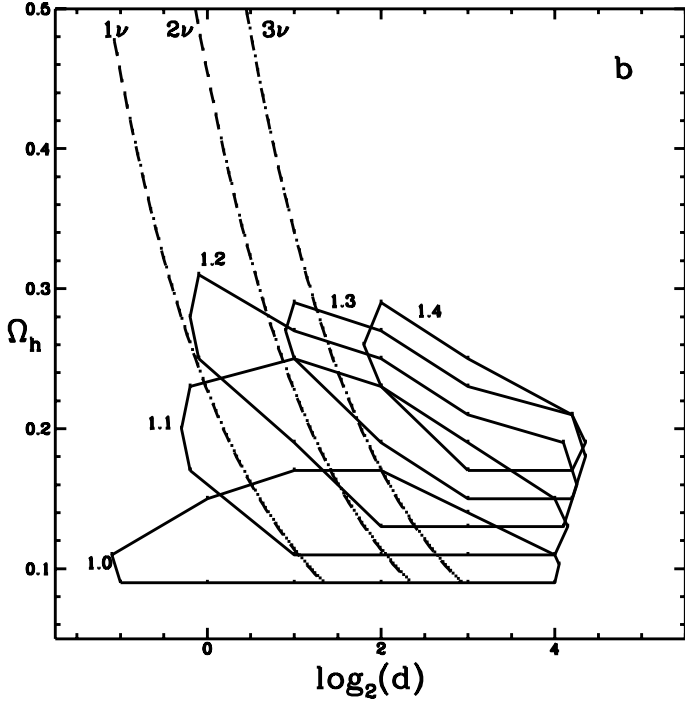


Figure 1. Parameter constraints from LSS. Dashed lines refer to neutrino cases with 1, 2 and 3 massive neutrinos (from left to right). Solid lines are the contours of the regions allowed in volatile models for different values of n (marked next to the arcs). The plot refers to $\Omega_b = 0.1$. The constraints considered are the shape parameter Γ , the σ_8 and the number density of clusters are considered (see BP for a detailed discussion).

from a pure Friedmann metric, due to gravitational field inhomogeneities, are given by the *potentials* Ψ and Φ .

In the presence of inhomogeneities, the temperature of radiation $T(\hat{n}) = \langle T \rangle [1 + \Delta_T(\hat{n})]$ contains an anisotropy term, which can be thought as a superposition of plain waves of wave-numbers \vec{k} . In respect to a given direction \hat{n} , the amplitude of the single \vec{k} mode can be expanded into spherical harmonics. For our statistical aims it is however sufficient to consider the anisotropy as a function of $\mu = \hat{k} \cdot \hat{n}$ and use the expansion:

$$\Delta_T(\vec{k}, \hat{n}, \tau) = \sum_{l=0}^{l=\infty} (-i)^l (2l+1) \Delta_l(\vec{k}, \tau) P_l(\mu), \quad (3.2)$$

where P_l are Legendre polynomials and whose coefficients can be used to work out the angular fluctuation spectrum

$$C_l = (4\pi)^2 \int dk k^2 P_\psi(k) |\Delta_l(\vec{k}, \tau)|^2 \quad (3.3)$$

which, for a gaussian random field, completely describes angular anisotropies.

At the present time τ_o and for a comoving scale given by the wavenumber k , we can compute Δ_l performing a time integral (Seljak and Zaldarriaga, 1996)

$$\Delta_l(k, \tau_o) = \int_0^{\tau_o} dx S(k, \tau) j_l[(\tau_o - \tau)k] \quad (3.4)$$

over the source function S , which depends upon inhomogeneity evolution inside the last scattering band and from it to now.

generality evolution inside the last scattering band and from it to now.

The physics of microwave background anisotropies due to adiabatic perturbations has been deeply investigated in the last few years.

It has been shown that the characteristics of the peaks in the C_l spectrum are related to the physics of acoustic oscillations of baryons and radiation between the entry of a scale in the horizon and the last scattering band, and on the history of photons from last scattering surface to us.

Background features, like the overall matter and radiation density content, h and Λ , have an influence both on the positions of the peaks and on their amplitude, but the latter also depends greatly on the baryon content Ω_b and more slightly on the characteristic of the hot component.

In the following we shall analyze in detail the angular spectrum of volatile models, outlining its peculiarities with respect to standard CDM and neutrino models. In order to do so, we need to modify available public codes, like CMBFAST, allowing them to deal with a hot component whose momentum distribution is (2.6).

It should also be recalled that volatile and neutrino models, for given Ω_h and d , are expected to include a different amount of SMLC. In neutrino models SMLC is less than in pure CDM and even vanishes if all ν 's are massive (unless extra SMLC is added *ad hoc*). In volatile models, instead, SMLC is however more than in pure CDM, as scalar ϕ 's are added on top of standard massless ν 's.

Several C_l spectra of volatile models are presented in figs. 6–15. They show two main features, if compared with standard CDM: the first doppler peak is higher and the second and third doppler peaks are slightly shifted to the right.

In principle, we expect volatile model spectra to differ from neutrino model spectra because of the momentum distribution of volatiles and the extra SMLC they have to include. In the following, we shall try to disentangle these two effects.

To this aim we coupled each volatile models with a *technical* neutrino case with identical Ω_h and d , but a greater number of neutrino degrees of freedom, so to ensure equal high-redshift energy densities. In fig. 2 we report the scale-factor dependence of the energy densities $\rho(a)$ of volatiles and a massive neutrinos in two coupled models. In the case shown, the two energy densities never differ in ratio more than 10^{-3} ; for different choice of the parameters the curve is just shifted to higher or lower redshifts according to the value of z_{der} .

More in detail fig. 2 states that volatiles have a slower derelativization than neutrinos: the transition phase from the relativistic to the non-relativistic regime starts earlier and goes on for a longer time. This behaviour is related to the different shapes of the two distribution functions, and to the fact that the volatile one is smoother around $\langle p \rangle$, which corresponds to a value significantly smaller than its maximum, after which it is rapidly cutoff [see eqs. (2.6), (2.7)].

Friedman equations show that $\tau(a)\sqrt{\rho(a)}$ is approximately constant. Hence, once we know $\rho(a)$, we can perform a comparison between the conformal times of coupled volatile and *technical* neutrino cases. It shows a marginal discrepancy as already the $\rho(a)$ in the volatile and *technical* neutrino cases are very similar, and moreover the hot com-

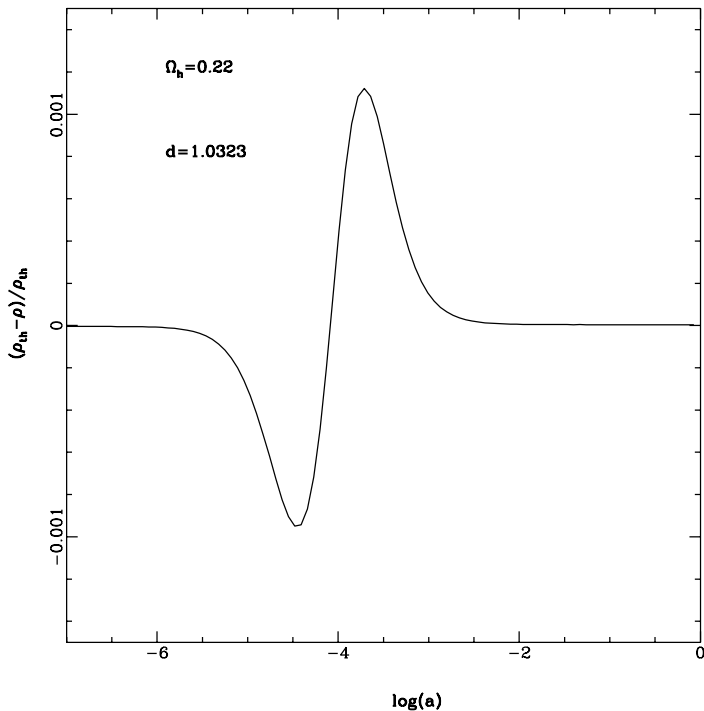


Figure 2. density evolution of a volatile model in comparison with the corresponding technical neutrino case.

ponent always contributes as a small fraction of the total energy density. On the contrary, if a similar comparison is performed between standard CDM and volatile models, big discrepancies are found, especially at high redshifts. In fact, in the volatile cases the relativistic background is greater due to the contribution of the sterile component, and the conformal time is therefore smaller than in the CDM case (see fig. 3). This implies visible effects on the position of the doppler peaks, which are due to the oscillatory phase with which the photon–baryon fluid meets the last scattering band (see Hu & Sugiyama 1995). The photon–baryon fluid oscillates as $\cos(kr_s)$, where k is the comoving scale and r_s is the sound horizon ($r_s = \int_0^{\tau(a)} d\tau c_s(a)$, $c_s(a)$ is the sound speed). Given the photon–baryon ratio, $r_s(a)$ follow a similar trend as $\tau(a)$. Since in volatile models $\tau(a)$ is smaller than in CDM, so will be $r_s(a)$, and the peaks of the spectrum will appear in correspondence to higher k (i.e. higher l) values.

This is a specific feature of these models, in neutrino models the same effect plays a role, but shifting the peaks in the opposite direction (Dodelson et al. 1996).

For a given n , the height of the peaks is fixed by (i) the ratio between baryon and photon densities, i.e. $\Omega_b h^2$, and (ii) the ratio between matter and radiation densities. At fixed Ω_b and h the main reason for a higher doppler peak in volatile models (with respect to CDM) is the delayed matter–radiation equivalence, for which both SMLC and, possibly, volatiles can be responsible. In neutrino models without *ad-hoc* SMLC, only the possible delay due to late derelativizing ν 's may exist. This is why volatile C_l spectra and standard neutrino ones look so different. However,

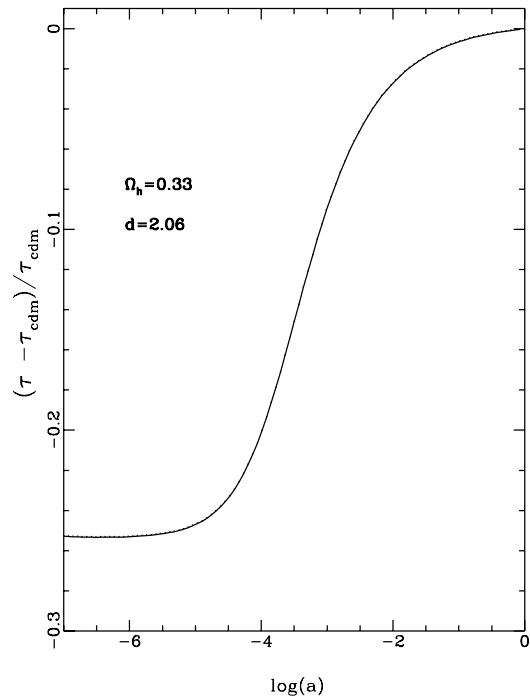


Figure 3. comparison of conformal time in a CDM standard model and in a volatile model. At high redshifts, volatile models typically show a smaller conformal time.

there is a tiny further contribution in the boost of the peak due to the free-streaming of the hot component. Several authors (Ma & Bertschinger 1995, Dodelson et al. 1996) have shown that even in high z_{der} neutrino models the doppler peaks are enhanced with respect to CDM, and in that case the free-streaming of the hot component is to be considered responsible for the enhancement. Free-streaming, in fact, causes a decay in the potential Φ which contributes as a forcing factor (through $\ddot{\Phi}$) in the equations whose solution are the *sonic* oscillations in the photon–baryon fluid, displacing their zero–point and, henceforth, the phase by which they enter the last scattering band. In the standard neutrino case, this effect causes a variation of 10% at most on the C_l , and typically of 2% on the first doppler peak.

In principle one can expect that the different momentum distribution of volatiles may alterate the free–streaming behaviour. Such differences, if they exist, can be found by comparing volatile spectra with the *technical* neutrino ones. The differences between the two spectra are presented are shown in fig. 4, and amount to 2% at most. Although modest, this is another feature that characterizes volatile models with respect to neutrino one.

In comparison with such finely tuned predictions from theoretical models, currently available data are still affected by huge errorbars. However, some feature seems already evident from them. In fig. 6–15 we perform a comparison of model predictions with data and show that the doppler peak observed by the Saskatoon experiment (Netterfield et al. 1997) exceeds the one expected in pure CDM once it is normalized to COBE data (Bennet et al. 1996). While it is evident that volatile models show a higher doppler peak,

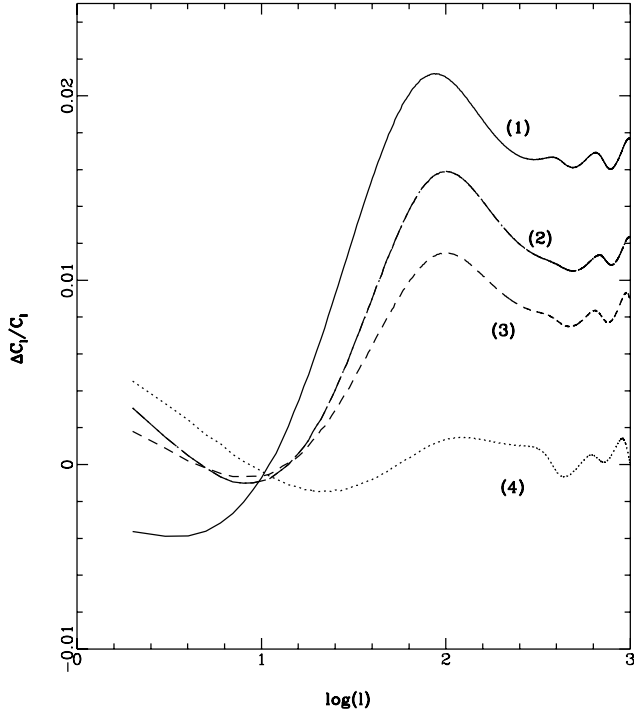


Figure 4. differences in the radiation power spectrum between the volatile case and the technical neutrino case. The model parameters are the following: 1) $\Omega_h = 0.16$, $d = 4.25$; 2) $\Omega_h = 0.22$, $d = 1.03$; 3) $\Omega_h = 0.22$, $d = 2.06$; 4) $\Omega_h = 0.33$, $d = 2.06$.

it is clear that a fit could be reached also changing other parameters, *e.g.*, by taking $n > 1$. In fig. 4 we show what happens in neutrino models if the spectrum is anti-tilted to $n = 1.1$ and to $n = 1.2$. Indeed, the first doppler peak is raised (which is desirable), but also the following peaks are raised, making difficult the agreement with the results from the CAT experiment (Scott et al. 1996). In section 5 similar considerations will be used in order to constrain the whole set of volatile models.

4 CONSTRAINTS FROM LARGE SCALE STRUCTURE

Mixed model parameters can be constrained from particle physics and/or from LSS. In this section we review a number of the latter constraints, which can be tested without discussing non-linear evolution. In Appendix A we debate constraints on the spectral index n arising from inflation.

Even without considering their non-linear evolution, models can be constrained through the following prescriptions:

(i) The numerical constant A_Ψ , in the spectrum (1.1), must give a value of C_2 consistent with the COBE quadrupole $Q_{rms,PS}$. Values of A_Ψ consistent with the $Q_{rms,PS}$ values, for a given n , within 3σ 's, can be kept.

(ii) COBE quadrupole therefore fixes the normalization at small k . The first large k test to consider, then, is the behaviour on the $8h^{-1}$ Mpc scale. Quite in general, the mass

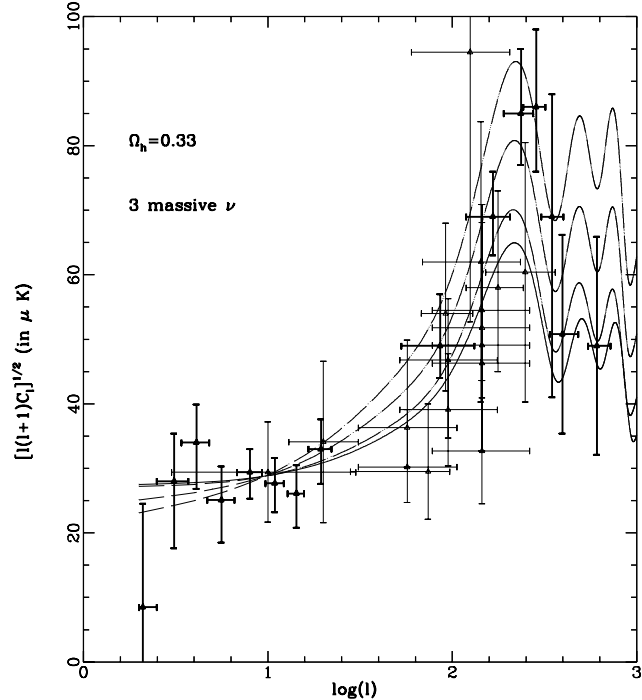


Figure 5. a standard neutrino model with different n values. C_l curves from bottom to top correspond to $n = 1, 1.1, 1.2, 1.3$. Bold data points refer to COBE (Tegmark 1996), CAT (Scott et al 1996), Saskatoon (Netterfield et al. 1997); see Scott et al (1995) for a summary of all the experiments.

M_λ , within a sphere of radius $L = \lambda h^{-1}$ Mpc, is

$$M_\lambda = 5.96 \cdot 10^{14} \Omega_h^2 M_\odot (\lambda/8)^3. \quad (4.1)$$

Therefore, the $8h^{-1}$ Mpc scale is a typical cluster scale. Here optical and X-ray data are to be exploited to work out the mass variance σ_8 and models should fit such observational outputs. Optical data provide the cluster mass function through a virial analysis of galaxy velocities within clusters. X-ray determinations, instead, are based on observational temperature functions. If clusters are substantially virialized and the intracluster gas is isothermal, the mass M of a cluster can then be obtained, once the ratio $\beta_{th,gal}$ between thermal or galaxy kinetic energy (per unit mass) and gravitational potential energy (per unit mass) is known. Values for β 's are currently obtained from numerical models.

Henry & Arnaud (1991) compiled a complete X-ray flux-limited sample of 25 clusters which is still in use for such determinations. Assuming an isothermal gas, full virialization and $\beta \equiv \beta_{gal}/\beta_{th} = 1.2$ they had estimated $\sigma_8 = 0.59 \pm 0.02$. Their error does not include β uncertainty. Various authors then followed analogous patterns (see, *e.g.*, White et al. 1993, Viana & Liddle 1996). Recently Eke et al. (1996) used Navarro et al. (1995) cluster simulations to take $\beta = 1$ with an error $\lesssim 6\%$. Accordingly they found $\sigma_8 = 0.50 \pm 0.04$. By comparing the above results one can estimate that, to obtain $\sigma_8 \sim 0.7$, under the assumption of full virialization and purely isothermal gas, $\beta \sim 1.4$ is needed.

An estimate of cluster masses independent from clus-

ter models can be obtained by comparing optical and X-ray data. Recent analyses (Girardi et al. 1998) seem to indicate values of $\beta \simeq 0.88$. In our opinion, such outputs do not strengthen the case of a safe cluster mass determination, as they are more than 12 % below Navarro et al. (1995) ratio and might indicate a non equilibrium situation. Furthermore, it ought to be outlined that cluster mass determinations based on a pure virial equilibrium assumption conflict with the observed baryon abundances and would require cosmological models with $\Omega_b \sim 0.16$ – 0.20 , in contrast with BBNS constraints, if all dark matter is CDM and $\Omega = 1$.

If HDM is only partially bound in clusters and their masses are underestimated by ~ 15 – 20 %, the latter conflict can be overcome. (Alternative way outs, of course, are that $\Omega < 1$ or $\Lambda \neq 0$.) Therefore, in order that data be consistent with mixed models, some mechanism should cause a slight but systematic underestimate of cluster masses. Owing to such uncertainties, we can state that cluster data constrain σ_8 within the interval 0.46 – 0.70 .

These constraints can also be expressed with direct reference to the cumulative cluster number density. Defining the mass $M(u)$ for which the top-hat mass variance $\sigma_{M(u)} = \delta_c/u$ (here δ_c values from 1.55 to 1.69 can be considered) the Press & Schechter approach yields the number density

$$n(> M) = \sqrt{2/\pi}(\rho/M) \int_{\delta_c/\sigma_M}^{\infty} du[M/M(u)] \exp(-u^2/2) . \quad (4.2)$$

A usual way to compare it with data amounts to taking $M = 4.2h^{-1} \cdot 10^{14}M_{\odot}$ and considering then $N_{cl} = n(> M)(100h^{-1}\text{Mpc})^3$ for the above M value. With a range of uncertainty comparable with the one discussed for σ_8 , optical and X-ray data converge towards a value of $N_{cl} \sim 4$. Henceforth viable models should have $1 \lesssim N_{cl} \lesssim 10$, for one of the above values of δ_c .

There is a slight difference between testing a model in respect to σ_8 or N_{cl} . This amounts to the different impact that the slope of the transferred spectrum has on expected values. Observations, however, also constrain the observed spectral slope, as we shall detail at the point (iv).

(iii) In order to have N_{cl} and σ_8 consistent with observations, the A_{Ψ} interval obtained from COBE quadrupole may have to be restricted. The residual range of A_{Ψ} values can then be used to evaluate the expected density of high- z objects, that mixed models risk to *under-produce*. The most restrictive constraints comes from computing $\Omega_{\text{gas}} = \alpha\Omega_b\Omega_{\text{coll}}$ in damped Lyman α systems (for a review see Wolfe, 1993).

It can be shown that

$$\Omega_{\text{coll}} = \text{erfc}[\delta_c/\sqrt{2}\sigma(M, z)], \quad (4.3)$$

where $\sigma(M, z)$ is the (top hat) mass variance (for mass M at redshift z) and α is an efficiency parameter which should be $\lesssim 1$. More specifically, using such expression, one can evaluate $D_{Las}(M, z) \equiv \Omega_{\text{gas}} \times 10^3/\alpha$. Then, taking $z = 4.25$, $\delta_c = 1.69$ and $M = 5 \cdot 10^9 h^{-1}M_{\odot}$ we have a figure to compare with the observational value given by Storrie-Lombardi et al. (1995): $D_{Las} = 2.2 \pm 0.6$.

Only models for which the predicted value of D_{Las} exceeds 0.5 , at least for a part of the allowed A_{Ψ} interval, are

therefore viable. In turn, also for viable models, this may yield a further restriction on the A_{Ψ} interval.

(iv) Models viable in respect to previous criteria should also have a fair slope of the transferred spectrum. Its slope can be quantified through the *extra-power* parameter $\Gamma = 7.13 \cdot 10^{-3}(\sigma_8/\sigma_{25})^{10/3}$ ($\sigma_{8,25}$ are mass variances on the scales $R = 8, 25 h^{-1}\text{Mpc}$). Using APM and Abell/ACO samples Peacock and Dodds (1994) and Borgani et al. (1997) obtained Γ in the intervals 0.19 – 0.27 and 0.18 – 0.25 , respectively. Such intervals essentially correspond to 2σ 's. Furthermore the lower limit can be particularly sensitive to underestimates of non-linear effects. Henceforth, models yielding Γ outside an interval 0.13 – 0.27 are hardly viable.

One can also test models against bulk velocities reconstructed POTENT from observational data. This causes no constraint, at the 2σ level, on models which survived previous tests.

In BP a number of plots of the transferred spectra of viable models, were shown against LCRS reconstructed spectral points (Lin et al. 1996). However, previous constraints include most quantitative limitations and models passing them fit spectral data. Fig. 1 is taken from BP and reports the curves on the Ω, d plane limiting areas where viable mixed models exist for various primeval n values, if $\Omega_b = 0.1$. All models considered in the next sections, both for $\Omega_b = 0.1$ and $\Omega_b = 0.05$, were previously found to satisfy the above constraints.

5 CMB DATA AND PARAMETER SPACE LIMITATION

In this section we give the CBR spectra of the hot-volatile models and compare them with available data, ranging from $l = 2$ to $l \lesssim 500$.

We evaluated the spectra for several parameter choices allowed by LSS constraints (see fig. 1). Significant example of C_l spectra are shown in figs.6–15 while the corresponding LSS predictions are summarized in table 1.

Some parameter sets are compatible with neutrino hot dark matter, while models with a low z_{der} and $n_{\gamma} \gtrsim 1$ are obtainable with volatile hot dark matter. Since the height of the first doppler peak is very sensitive to the baryon abundance, we considered two values of Ω_b , namely 0.05 and 0.1 . Spectra are normalized to $Q_{rms,PS}$ assuming no contribution of gravitational waves. As is known, their contribution would raise the low- l tail of the C_l spectrum, therefore reducing the gap between the Sacks-Wolfe *plateau* and the top of the first doppler peak.

Models with $\Omega_b = 0.1$ systematically show a peak less pronounced than models with $\Omega_b = 0.05$. It is well known that models with a given h and hot component show a lower doppler peak for smaller Ω_b ; in top of that, here there is a further effect: LSS constraints often are compatible with a part of the observational $Q_{rms,PS}$ interval, and low Ω_b models tend to be consistent with low $Q_{rms,PS}$ values.

While in fig. 5 we plot most data are available, in figs.6–15 we compare models with data from COBE (Tegmark 1996) Saskatoon (Netterfiled et al. 1997) and CAT (Scott et al. 1996) only.

Figs. 6–15 show a systematic trend: for a given large l value, C_l increases with both n and $d = 10^4/z_{der}$. On the

[h]

Table 1. Model parameters and power spectra. Column 1: volatile fractional density; Column 2: redshift at which the volatile component becomes non-relativistic ($d = 10^4/z_{der}$); Column 3: total number of equivalent massless neutrinos ($n_\nu = g_{\nu,eff}/2$); Column 4: n value considered; Columns 5–7: Large scale structure predictions.

Ω_h	d	n	N_ν	σ_8	Γ	$N(> M)$
$\Omega_b = 0.05$						
0.11	8	1	6.9	0.53–0.68	0.23	1.8–9.8
0.11	8	1.1	6.9	0.63	0.27	6.9
0.16	2.83	1	5	0.60–0.68	0.20	4.0–9.3
0.16	2.83	1.1	5	0.67	0.24	8.9
0.11	16	1.1	10.7	0.52–0.64	0.24	1.6–7.3
0.19	8	1.1	9.7	0.55–0.66	0.16	2.0–7.7
0.19	8	1.2	9.7	0.55–0.67	0.19	2.1–8.1
0.20	4	1.2	6.5	0.67	0.20	8.3
0.24	4	1.3	7.2	0.64–0.69	0.17	6.4–9.4
0.23	8	1.3	8.9	0.57–0.68	0.17	2.7–9.3
$\Omega_b = 0.1$						
0.11	8	1	6.9	0.52–0.65	0.21	1.4–7.6
0.11	8	1.1	6.9	0.58–0.67	0.24	3.6–8.9
0.16	2.83	1	5	0.66–0.68	0.18	7.4–9.0
0.16	2.83	1.1	5	0.60–0.65	0.21	4.4–7.1
0.11	16	1.1	10.7	0.47–0.67	0.22	1.0–7.9
0.19	8	1.1	9.7	0.57–0.68	0.14	2.9–8.7
0.19	8	1.2	9.7	0.49–0.67	0.17	1.0–8.0
0.20	4	1.2	6.5	0.66–0.68	0.13	7.1–8.0
0.24	4	1.3	7.2	0.54–0.69	0.14	1.6–8.8
0.23	8	1.3	8.9	0.52–0.70	0.15	1.2–10

contrary, for a given large k value, the matter fluctuation spectrum $P(k)$ increases with n but is damped for large d , so that these to effects tends to compensate.

This is one of the reasons why LSS constraints can be compatible with n as high as 1.4. On the contrary, figs.14–15 show that CBR spectra already disfavour $n = 1.3$ if $d \gtrsim 4$ ($z_{der} \lesssim 2500$) is considered, no matter the value of Ω_b . Volatile models with $n > 1.2$ are largely out of the errorbars, and should be considered as scarcely viable. Nevertheless, even for $n = 1.2$, volatile models allow a higher first doppler peak without raising the following ones, and therefore fit the data better than neutrino models. Just as large n , also large d causes conflict with data, by itself. For example, fig. 10 show that models with $d = 16$ are disfavoured, even with low Ω_h and $n = 1.1$.

As pointed out in section 2, volatile models require a sterile component whose energy density is proportional to $\Omega_h d$. Its effective number of degrees of freedom is linked to the equivalence redshift, which in turn affects both the shape parameter Γ and the height of the first doppler peak. Dodelson et al. (1994) considered the matter power spectrum in the case of a τ -neutrino decay (τ CDM model), and found that even in that case the effective number of degrees of freedom $g_{\nu,eff}$ is bigger than in standard CDM. They outlined that, in order to lower Γ at least down to 0.3 (Peacock & Dodds 1994), in a $h = 0.5$ universe with $n = 1$, an equivalent number of massless neutrinos as high as 16 is needed.

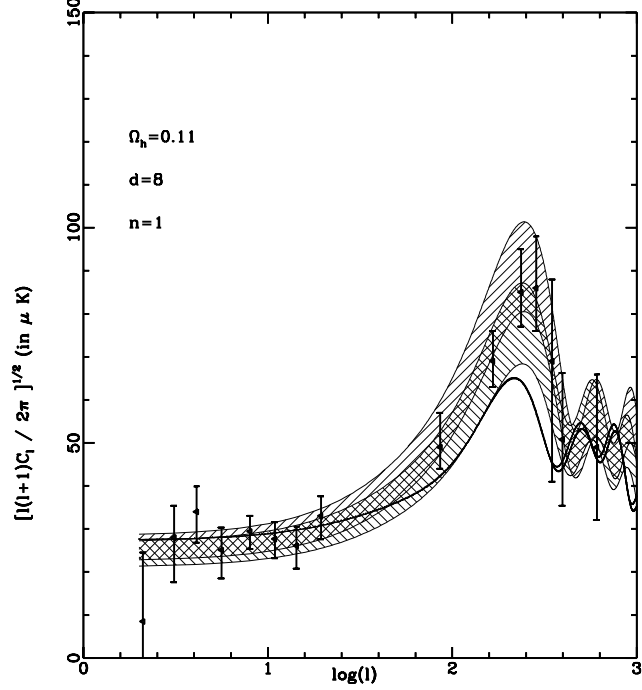


Figure 6. volatile spectra are compared with the observational data from COBE, Saskatoon and CAT experiments. The errorbars correspond to 1σ errors. Solid bold lines refer to standard CDM ($h = 0.5$, $n = 1$, $\Omega = 1$) and a neutrino model with $\Omega_h = 0.3$. Shaded areas are the volatile spectra with parameters specified in the figure. Upward shading refers to $\Omega = 0.1$ models while downward shading to $\Omega = 0.05$. Notice that $z_{der} = 10^4/d = 1250$.

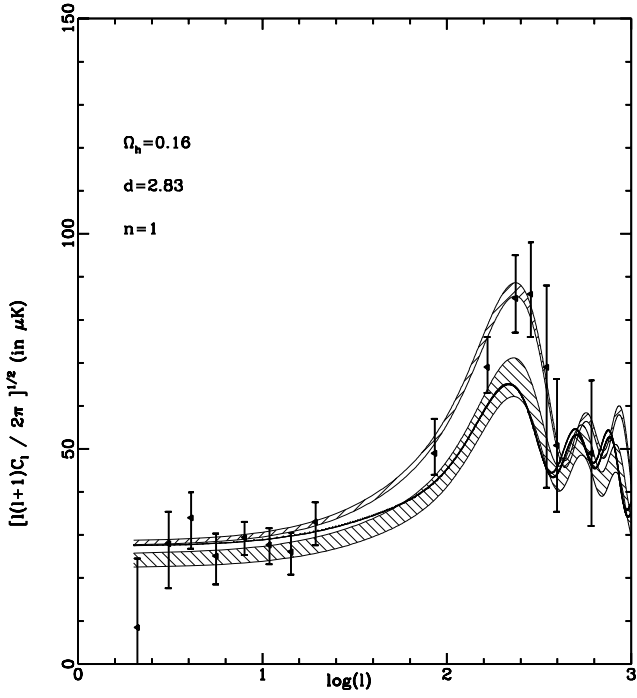
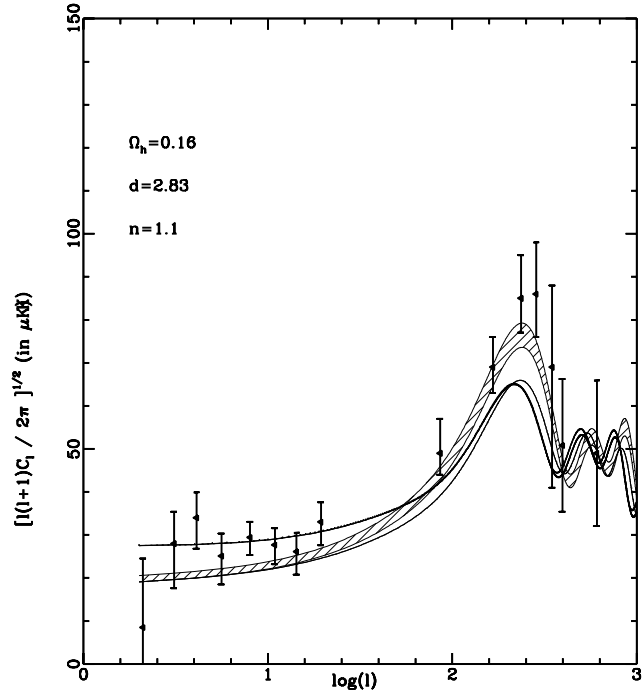
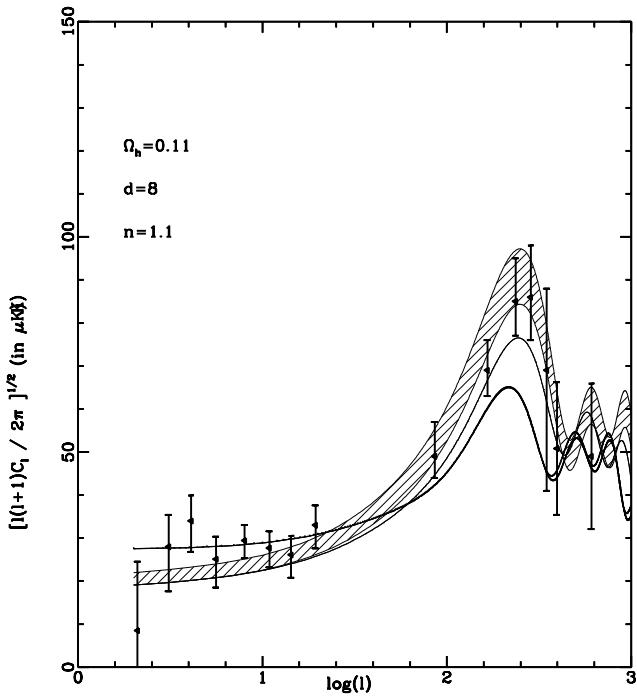
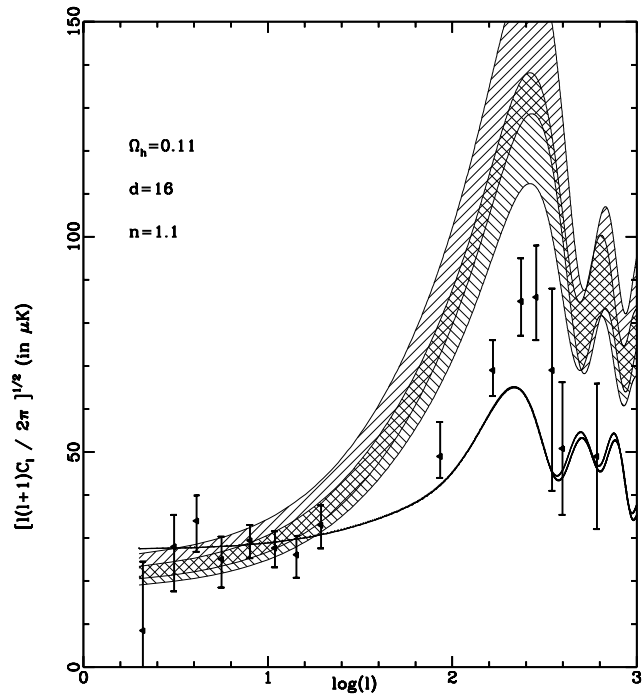
White et al. (1995), who also consider τ CDM models but with a lighter neutrino, also pointed out that the predicted Γ of these models is lower due to the high $g_{\nu,eff}$, and show that a lower Γ implies a higher first doppler peak. Their work, however, is only qualitative, and they don't infer any restriction in the parameter space using the data. Looking at the data, we found out that if $n = 1.1$, CBR data models with an equivalent number of neutrino species $N_\nu \gtrsim 10$ as in figs. 10, 12 and 15 are disfavoured. Models like the one shown in fig. 8 ($N_\nu \simeq 7$) seem to better fit the data, although even lower N_ν ($\simeq 5$), as provided by the model in fig. 9, should not be disregarded.

Keeping to $n = 1$, LSS already exclude very high $\Omega_h d$ values, so that a low N_ν is automatically ensured. The models shown in figs. 6–7 seem to well fit the data, with a corresponding $N_\nu = 5 - 7$.

6 CONCLUSIONS

In this work we have analyzed mixed models from the point of view of both LSS and CMB predictions. We considered different hot dark matter components: the standard neutrino case and the volatile case in which particles come from the decay of heavier ones.

First we tested the mixed models on available LSS data requiring fair predictions for σ_8 , Γ , DLAS and N_{cl} . This

Figure 7. volatile spectra compared to the data. $z_{der} = 3533$.Figure 9. volatile spectra compared to the data. $z_{der} = 3533$.Figure 8. volatile spectra compared to the data. $z_{der} = 1250$.Figure 10. volatile spectra compared to the data. $z_{der} = 625$.

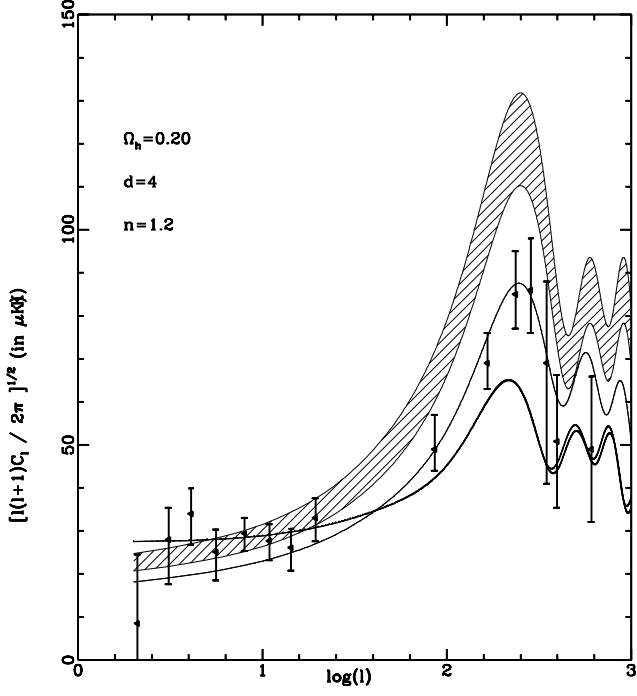


Figure 11. volatile spectra compared to the data. $z_{der} = 2500$.

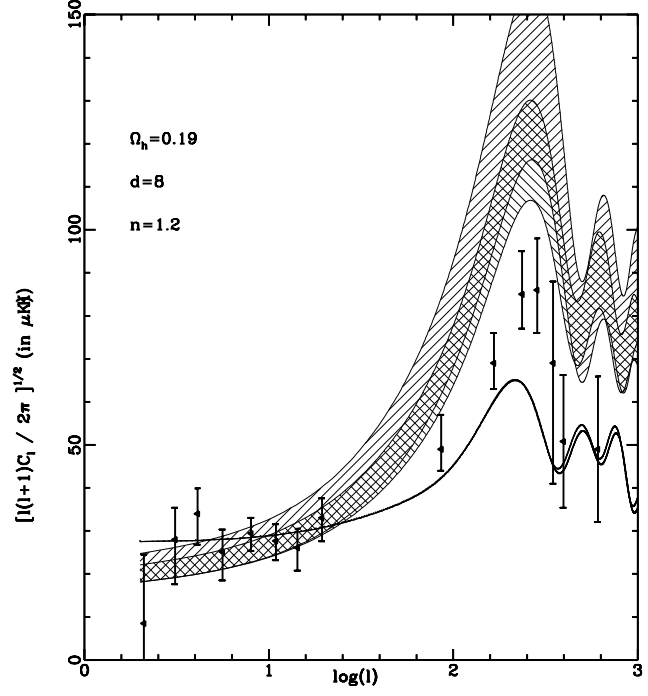


Figure 13. volatile spectra compared to the data. $z_{der} = 1250$.

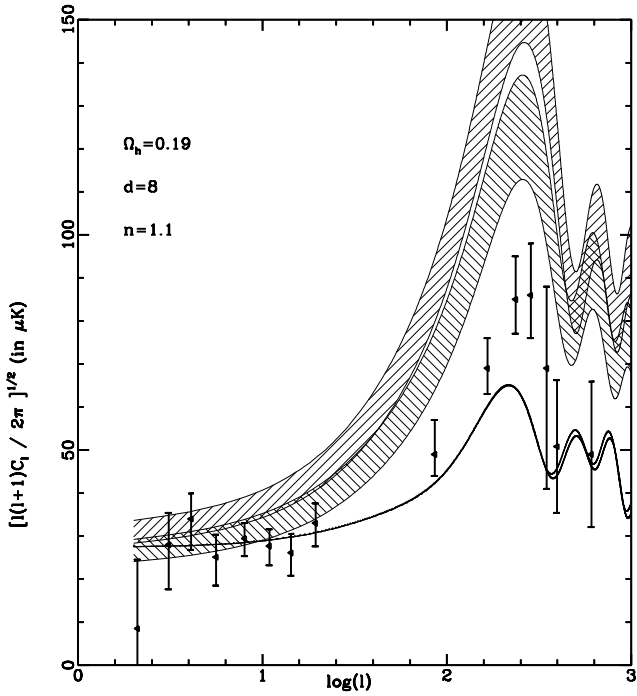


Figure 12. volatile spectra compared to the data. $z_{der} = 1250$.

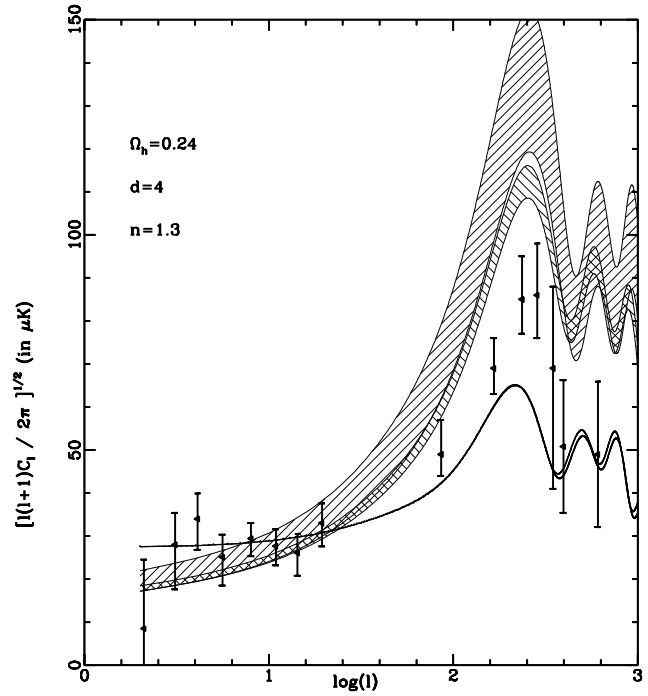


Figure 14. volatile spectra compared to the data. $z_{der} = 2500$.

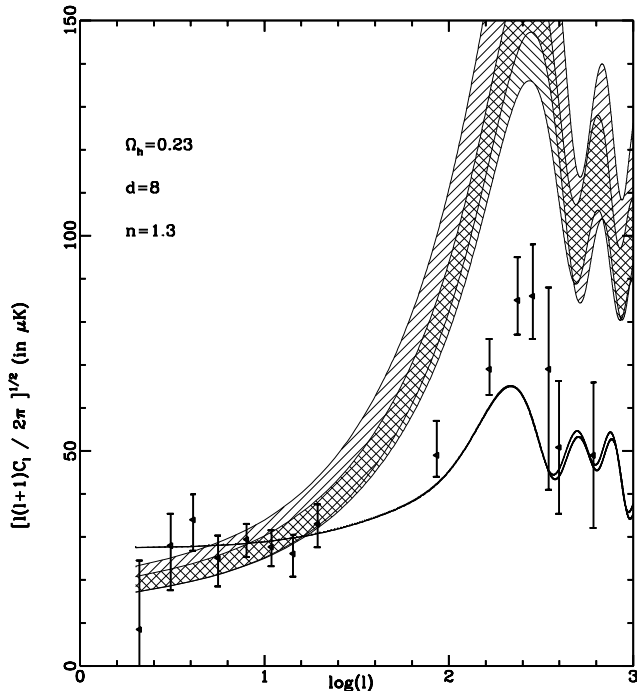


Figure 15. volatile spectra compared to the data. $z_{der} = 1250$.

analysis shows that it must be $\Omega_h \lesssim 0.3$. This comes as no surprise, as mixed models with greater Ω_h have not been considered since long. The new result is that taking n up to 1.4 does not ease the problems previously found for large Ω_h .

On the contrary, volatile models together with $n > 1$ significantly widen the parameter space in the low z_{der} direction and viable models even with $z_{der} \sim 600$ can be found. In fact, as far as $P(k)$ is concerned, we found a nearly degenerate behaviour of the parameters n and z_{der} , as the damping on the high k values due to low z_{der} can be compensated by high n .

CBR data, apparently, break the degeneracy. In section 3 we have shown that the CBR spectrum of volatile models is significantly different from standard CDM and also from neutrino models usually considered. In fact SMLC and late z_{der} volatiles cause a late z_{eq} and, henceforth, a higher first doppler peak. Minor effects are caused by the typical momentum distribution of volatiles. These effects amounts to 2% at most in the C_l spectrum and only an accurate analysis of the results of future satellites, as MAP and Planck, could allow to detect it.

CBR spectra of volatile models were then compared with available data from different experiments, namely those from COBE, Saskatoon and CAT experiments. Data on CBR spectrum at large l imply that temperature fluctuations $\Delta T/T \sim 10^{-5}/l$ are appreciated. Therefore, measures of the CBR spectrum, for high l values, still need to be treated with some reserve. It seems however clear that recent observations tend to indicate a doppler peak higher than expected both for pure CDM and for mixed models with early derelativization, such as most neutrino models.

Taking $n > 1$ and/or late derelativization raises the doppler peak and affects the CBR spectrum at high l . The first question we tried to answer is how far we can and have to go from pure CDM and $n = 1$ to meet current large l data.

We found that volatile models could cure this discrepancy, while ensuring a viable scenario for structure formation.

In turn, large l data imply restrictions in the parameter space, complementary to the ones derived from LSS while a fit of such data requires only a slight departure from pure CDM and $n = 1$. allows us to say that mixed models are in very good shape. For example, fig.s 8-9 show the C_l behaviour for $n = 1.1$ and HDM ranging from 11% to 16%. Such models provide excellent fits to current data and, as explained in BP, are also in agreement with LSS.

Other models, for larger n and Ω_h or lower z_{der} , show only a marginal fit with current observations. Hopefully, future data on high l 's will be more restrictive and allow safer constraints. At present, such models cannot be ruled out, although they are more discrepant from pure CDM and $n = 1$ than high l data require.

In our opinion, however, CBR data can already be said to exclude a number of models which fitted LSS data. In general, models with $n > 1.3$ and $z_{der} < 1000$ seem out of the range of reasonable expectations.

Altogether, three kinds of departures from CDM and Zel'dovich were considered in this work: large Ω_h , low z_{der} and $n > 1$. Large (but allowed) Ω_h values, by themselves, do not ease the agreement of models with high l data. Taking $n > 1$ eases the agreement of models with data for $l \sim 200$, as is expected, but seems to rise the angular spectrum above data for greater l 's. Taking low z_{der} , instead, raises the doppler peak, but does not spoil the agreement with greater l data. Current data, therefore, seems to support models with a limited amount of HDM or volatile materials, possibly in association with n slightly above unity, to compensate some effects on LSS.

Note that the analysis of this work is carried out keeping $h = 0.5$, allowing for no cosmological constant, and constraining the total density to be critical. E.g., raising h would probably allow and require a stronger deviation from pure CDM and $n = 1$. We plan to widen our analysis of the parameter space in the near future, also in connection with the expected arrival of fresh observational data on the CBR spectrum.

ACKNOWLEDGMENTS

E.P. wishes to thank the University of Milan for its hospitality during the preparation of this work.

REFERENCES

- Bartlett J.G., Blanchard A., Le Dour M., Douspis M., Barbosa D., 1998, astro-ph/9804158
- Bennet C.L. et al., 1996, ApJ 464, L1
- Bond J.R., Efstathiou G., 1991, Phys. Lett., B265, 245
- Bonometto S.A., Gabbiani F. and Masiero A., 1994, Phys.Rev. D49, 3918
- Bonometto S., Pierpaoli E., 1998, New Astronomy (in press)

- Borgani S., Moscardini L., Plionis M., Górski K.M., Holzman J., Klypin A., Primack J.R., Smith C.C. and Stompor R., 1997, *New Astr.* 321, 1
- Borgani S., Masiero A., Yamaguchi M., 1996, *Phys. Lett.*, B386, 189
- Copeland E.J., Liddle A.R., Lyth D.H., Stewart E.D. and Wands D., 1994, *Phys.Rev.* D49, 6410
- de Bernardis P., Balbi A., De Gasperis G., Melchiorri A., 1997, *ApJ* 480, 1
- De Gasperis G., Muciaccia P.F., Vittorio N., 1995, *ApJ* 439, 1
- Dodson S., Gyuk G., Turner M.S., 1994, *Phys. Rev. Lett.* 72, 3754
- Dodson S., Gates E., Stebbins A., 1996, *ApJ* 467, 10
- Ghigna S., Borgani S., Tucci M., Bonometto S.A., Klypin A., Primack J.R., 1997, *ApJ* 479, 580
- Ghizzardi S., and Bonometto S.A., 1996, *A&A*, 307, 697
- Eke V.R., Cole S., Frenk C.S., 1996, *MNRAS* 282, 263
- Linde A., 1991a, *Phys.Lett* B249, 18
- Linde A., 1991b, *Phys.Lett.* B259, 38
- Girardi M., Borgani S., Giuricin G., Mardirossian F., Mezzetti M., 1998, *astro-ph/9804188*
- Hancock S., Rocha G., Lasenby A.N., Gutierrez C.M., 1998, *MNRAS* 294, L1
- Hannestad S., 1998, *astro-ph/9804075*
- Henry J.P., Arnaud K.A., 1991, *ApJ* 372, 410
- Hu W., Sugiyama N., 1995, *Phys. Rev.* D51, 2599
- Liddle A.R., Lyth D.H., Schaefer R.K., Shafi Q., Viana P.T.P., 1996, *MNRAS* 281, 531
- Lin H., Kirshner R.P., Shectman S.A., Landy S.D., Oemler A., Tucker D.L., Schechter P., 1996, *ApJ* 471, 617
- Lineweaver C., 1997, *astro-ph/9702040*
- Lineweaver C., Barbosa D., 1998, *A&A* 329, 799
- Lucchin F., Colafrancesco S., De Gasperis G., Matarrese S., Mei S., Mollerach S., Moscardini L. and Vittorio N., 1996, *ApJ* 459, 455
- Navarro J.F., Frenk C.S., White S.D.M., 1995, *MNRAS* 275, 720
- Ma C.P., Bertschinger E., 1995, *ApJ* 455, 7
- McNally S.J., Peacock J.A., 1995, *MNRAS* 277, 143
- Netterfield C.B., Devlin M.J., Jarosik N., Page L., Wollack E.J., 1997, *ApJ* 474, 47
- Peacock J.A. and Dodds S.J., 1994, *MNRAS* 267, 1020
- Pierpaoli E. and Bonometto S.A., 1995, *A&A* 300, 13
- Pierpaoli E., Coles P., Bonometto S.A. and Borgani S., 1996, *ApJ* 470, 92
- Pierpaoli E., Borgani S., Masiero A., Yamaguchi M., 1998, *Phys.Rev.* D57, 2089
- Scott D., Silk J., White W., 1995, *Science* 268, 829
- Scott P.F. et al., 1996, *ApJ* 461, L1
- Seljak U., Zaldarriaga M., 1996, *ApJ* 469, 437
- Smoot G.F. et al., 1992, *ApJ* 396, L1
- Storrie-Lambardi L.J., McMahon R.G., Irwin M.J. and Hazard C. (1995) *Proc. ESO Workshop on QSO A.L. & astro-ph/9503089*
- Tegmark M., 1996, *ApJ* 464, L38
- Viana P.T.P., Liddle A.R., 1996, *MNRAS* 281, 323
- White S.D.M., Efstathiou G., Frenk C., 1993, *MNRAS* 262, 1023
- White M., Gelmini G., Silk J., 1995, *Phys. Rev.* D51, 2669
- Zabludoff A.I., Huchra J.P., Geller M.J., 1990, *ApJS* 74, 1

APPENDIX A

7 INFLATIONARY MODELS YIELDING $N > 1$

This section is a quick review of results in the literature, aiming to show that there is a wide class of inflationary models which predict $n > 1$, but $\lesssim 1.4$.

During inflation, quantum fluctuations of the *inflaton* field φ on the event horizon give rise to density fluctuations. Their amplitude and power spectrum are related to the Hubble parameter H during inflation and to the speed $\dot{\varphi}$ of the *slow-rolling-down* process. The critical quantity is the ratio $W(k) = H^2/\dot{\varphi}$, where H and $\dot{\varphi}$ are taken when the scale $2\pi/k$ is the event horizon. It can be shown that

$$n = 1 + 2 \frac{d(\log W)}{d(\log k)} \quad (a.1)$$

and, if W (slowly) decreases with time, we have the standard case of n (slightly) below unity. Such decrease occurs if the downhill motion of φ is accelerated and an opposite behaviour occurs if $\dot{\varphi}$ decreases while approaching a minimum. The basic reason why a potential yielding such a behaviour seems unappealing, is that the very last stages of inflation should rather see a significant φ -field acceleration, ending up into a regime of damped oscillations around the true vacuum, when reheating occurs.

However, the usual perspective can be reversed if the reheating does not arise when an initially smooth acceleration finally grows faster and faster, but is triggered by an abrupt first order phase transition, perhaps due to the break of the GUT symmetry. Before it and since the Planck time, most energy resided in potential terms, so granting a vacuum-dominated expansion. This picture of the early cosmic expansion is the so-called *hybrid inflation*, initially proposed by Linde (1991a).

A toy-model to realize such scenario (Linde 1991b, 1994) is obtainable from the potential

$$V(\varphi, \chi) = (\mu^2 - \lambda\chi^2)^2 + 2g^2\varphi^2\chi^2 + m^2\varphi^2 \quad (a.2)$$

which depends on the scalar fields φ and χ , that we shall see to evolve slowly and fastly, respectively. If the *slow* field is embedded in mass terms, the potential reads

$$V(\chi) = M^2\chi^2 + \lambda\chi^4 + \Lambda^4 \quad (a.3)$$

where

$$\Lambda^4 = \mu^4 + m^2\varphi^2 \quad \text{and} \quad M^2 = 2(g^2\varphi^2 - \lambda\mu^2). \quad (a.4)$$

Eq. (a.3) shows that V has a minimum at $\chi = 0$, provided that $M^2 \geq 0$. If $M^2 < 0$, instead, the minimum is for $\bar{\chi} = \sqrt{-M^2/2\lambda}$, yielding μ when $\varphi = 0$.

Large φ values therefore require that χ vanishes and then the potential

$$V(\varphi, 0) = \mu^4 + m^2\varphi^2 \quad (a.5)$$

gives a Planck-time inflation, as V goes from an initial value $\sim t_{Pl}^{-4}$ to a value $\sim \mu^4$. The downhill motion of φ will decelerate as soon as the second term at the *r.h.s.* of eq. (a.5) becomes negligible, in respect to μ^4 , which acts as a cosmological constant. This regime breaks down when the critical value $\varphi_c = \sqrt{\lambda\mu/g}$ is attained. Then M^2 changes sign and the configuration $\chi = 0$ becomes unstable. We have then a

transition to the true vacuum configuration $\bar{\chi}$, which reheats (or heats) the Universe.

There are several constraints to the above picture, in order that at least 60 e-foldings occur with $\varphi > \varphi_c$ and fluctuations have a fair amplitude. They are discussed in several papers (see, *e.g.*, Copeland et al. 1994, and references therein) and cause the restriction $n \lesssim 1.4$.

It is fair to outline that *hybrid* inflation is not just one of the many possible variations on the inflationary theme. In spite of the apparent complication of the above scheme, it is an intrinsically simple picture and one of the few patterns which can allow to recover a joint particle–astrophysical picture of the very early Universe.